Selective Synthesis of Tungsten Carbide Phases W_2C and WC as Hydrogenation Catalysts

Patrick Bretzler,[a] Michael Huber,[a] Aditya A. Rane,[b] Rolf E. Jentoft,[b] Klaus Köhler*,[a] Friederike C. Jentoft* [b]

[a] *Department of Chemistry, Inorganic Chemistry, Lichtenbergstrasse 4 and Catalysis Research Center, Ernst-Otto-Fischer-Strasse 1, Technical University of Munich, 85747 Garching, Germany.*

[b] *Department of Chemical Engineering, 686 North Pleasant Street, University of Massachusetts Amherst, Amherst, MA 01003-9303, USA,*

* Corresponding authors E-mail: klaus.koehler@tum.de; fcjentoft@umass.edu

Abstract

Tungsten carbides are possible low-cost replacements for noble metal catalysts, but the role of different carbide stoichiometries (W_2C, WC) and their polymorphs for catalytic behavior is poorly understood. We develop a “dynamic, isothermal” carburization of WO_3 in a mixture of CH_4 and H_2 to control phase composition and catalytic properties. A design-of-experiments approach reveals that the key parameters are synthesis temperature (670 to 775 °C) and addition of silica as stabilizer (0 or 70 mol%). X-ray diffraction shows that the composition can be adjusted from 14 to 99 wt.% W_2C, complemented by WC and a small fraction of W metal. Crystalline domain sizes for W_2C are smaller than those of WC (≥10 nm), affording thermodynamic stabilization of W_2C in agreement with computational predictions (Shrestha et al., Chem. Mater. 2021, 33, 4606−4620). The amount of CO adsorbed scales with W_2C content, and so does the performance in butyraldehyde or toluene hydrogenation.

Keywords

Transition metal carbide; Solid-state reaction; High surface area; Surface energy; Phase control; Butanal; Butanol; Toluene; Methylcyclohexane; Design of experiments.

1. Introduction

The catalytic properties of Group 6 carbides were first reported 50 years ago [1], and the discovery of the platinum-like catalytic behavior of tungsten carbide by Levy and Boudart [2] led to the inception of the field of catalysis by transition metal carbides. The main advantage, then and today, is the material cost for tungsten, which is almost three orders of magnitude lower than for platinum [3].

Tungsten carbide was found to be active in hydrogenation reactions [2], hydrocarbon isomerization [2], hydrogenolysis [4,5], and methanol conversion [6]. Of recent interest is the ability of tungsten carbide to catalyze a number of reactions that aim to increase sustainability or provide efficient energy conversion. Upgrading of biomass has become a focus of carbide catalyst research. Hollak et al. [7] performed deoxygenation reactions of oleic acid on tungsten carbide catalysts, while Bitter and co-workers selectively deoxygenated several fatty acids [8–10] and guaiacol [11]. In addition Ren et al. [12] investigated the hydrodeoxygenation of short-chained aldehydes. Tungsten carbide is applied in the production of ethylene glycol from cellulose [13] and from sugars [14], and it has been used in the cracking of C–O bonds in lignin feedstock [15]. Together with nickel, tungsten carbide has been used for the ring opening of furfural [16]. Besides hydrogenation reactions, the material has attracted much attention as an electrocatalyst for the hydrogen evolution reaction, either as a support for platinum [17] or on its own [18,19]. In medium-temperature electrolysis, it can even rival the catalytic activity of platinum [20,21].

A pre-requisite for the economic use of tungsten carbide as catalyst is the preparation of materials with high surface area, which precludes the use of metallurgical methods. Added complexities are the existence of different tungsten carbide stoichiometries and phases, namely tungsten monocarbide (WC) and tungsten semicarbide (W_2C) with associated polymorphs, and the possible passivation of the surface by contaminants.

The goal of high surface area has been achieved by temperature-programmed carburizations, which initially started from tungsten nitride [22] and then from tungsten oxide [23]. The precursor is heated to a high temperature (700 °C – 900 °C) in a gas mixture of a carbon source (e.g., methane, ethane, ethene) and hydrogen [24,25]. If an oxide precursor is used, it is reduced, and carbon is inserted in several steps, forming a mixture of W_2C and WC. The properties of the produced tungsten carbide are highly dependent on the synthesis parameters [24,26].

There are several polymorphs of each of the two stoichiometries, WC and W_2C, with different stabilities. Unfortunately, there is confusion with the naming of these polymorphs, and the commonly made distinction by Greek letters is inconsistent. For a bulk material (thus not

considering contributions of surface energy), WC ($P\bar{6}m2$, $hP2$, WC type), often called δ-WC, is the thermodynamically favored phase below 1250 °C [27]. At higher temperatures, several W_2C phases become stable, labeled as α, β, γ or alternatively as β'', β', β; these phases have the same tungsten sublattice and are difficult to distinguish by X-ray diffraction.

During carburizations starting from oxides, phases with lower carbon content may be formed first, but these metastable, intermediate products are readily converted to WC in the presence of carbon [28]. Carbon chemical potential is obviously a factor in adjusting the carbide stoichiometry. During the synthesis with gaseous sources, amorphous carbon may be continuously deposited on the surface of the catalyst. This abundance of carbon gives little control over the tungsten carbide phase composition and easily results in the formation of the thermodynamically favored WC. Additionally, the deposited carbon can block the catalyst surface and has to be removed by a hydrogen treatment before catalysis [23,29].

The difficult synthesis of W_2C results in fewer investigations using this carbide phase, especially in the absence of a carbon support [30,31]. In a similar manner, the majority of theoretical works focus on WC while only a few include W_2C [32,33]. Although tungsten carbide catalysts have been under investigation for several decades and materials of both stoichiometries have been found catalytically active for hydrogenation reactions, the intrinsic activity of different carbide phases has not yet been resolved. In part, this lack of knowledge can be attributed to the difficulty to synthesize phase-pure materials.

A different synthesis approach has been developed to give better control of the carbide phase composition and avoid coking of the catalyst during synthesis. The use of a solid carbon support as carbon source slows down the carbon diffusion rate across the solid-solid interface and in turn, the carburization rate is limited. This method has been successfully employed over a range of carbon supports, from activated carbon [34] over carbon nanofibers [8] and multi-walled carbon nanotubes [31] to carbon spheres [35,36] as well as melamine [37] as organic precursor. Limiting the mobility and availability of carbon by binding it in a solid carbon matrix allows for the preparation of nanostructured and phase pure W_2C. The carbide synthesis still has to be managed carefully, as too low of a reaction temperature will result solely in the reduction of the tungsten precursor and the formation of metallic tungsten, while too high of a temperature will result in over-carburization and the formation of WC.

The use of a solid carbon source is not the only possible way to control the tungsten carbide phase composition. An alternative approach is the use of non-reducible oxides. Only few works are available on the effect of this type of oxide support on the carbide synthesis. Hunt et al. [38,39]

published the use of silica as a template to prepare small W_xC-nanoparticles. Hu et al. loaded tungsten oxide in the channels of silica SBA-15 by impregnation [40] as well as by a hydrothermal method [41] and successfully synthesized the carbide. Álvarez et al. [42] investigated the influence of aluminum addition in SBA-15 on tungsten carbide dispersion. Liu et al. [43] prepared tungsten oxide precursors on silica by an atomic layer deposition method and converted the tungsten oxide to tungsten carbide. In all cases, the metastable W_2C-phase was stabilized on the silica support for low tungsten loadings. This preference to W_2C was thought to result from different carbide formation processes dependent on the structure of the WO_x-sites in the precursor [41].

An alternative explanation for the stabilizing effect of a support is the high surface area imparted to the tungsten carbide. Stabilization of metastable phases for high surface area materials is well known for alumina, titania, and zirconia [44–46] and occurs at small crystal sizes, when a low surface energy renders particles of a high-bulk-energy phase thermodynamically more favorable relative to phases with a low bulk but high surface energy. Very recently, it has been proposed that this effect can alter the stability ranking of Group 6 carbide phases [33], but experimental evidence is scant.

The goals of the present investigation are (i) to first develop a synthesis method that allows control of the tungsten carbide phase composition, (ii) to characterize the materials and understand stability regimes of the different phases, and (iii) to identify structure-activity relationships in hydrogenation reactions.

To promote the formation of metastable W_2C during synthesis, we build on the reported effect of silica stabilizing this phase. A disadvantage of the typically employed temperature-programmed synthesis is that tungsten oxide reduction already starts before carbon insertion begins [24,25] and may progress to the metal for small precursor particles [47]. This pre-reduction possibly impedes the formation of a phase-pure tungsten carbide. Additionally, reports suggest that a higher surface area can be reached when the pre-reduction is prevented [48]. We present a new tungsten carbide synthesis method, in which the tungsten oxide is exposed to the reactive gas under isothermal conditions at the desired synthesis temperature. For this new method, the influence and interplay of synthesis temperature, synthesis time, precursor amount, use of silica as stabilizer and gas flow rate are examined. The parameters are varied in a design of experiments (DOE) two level fractional factorial plan [49]. This method maximizes the amount of useful information and verifies the statistical significance of the results. We demonstrate the robustness of the findings by transferring the synthesis to a different apparatus.

The catalysts are tested for their activity in two hydrogenation reactions, the conversion of butyraldehyde to butanol and the conversion of toluene to methylcyclohexane. Aromatic ring hydrogenations are structure sensitive on noble metals [50,51] and have the potential to provide additional insight about the catalytic behavior of different carbide surfaces.

2. Experimental Section

2.1. Materials

Chemicals were obtained from *Sigma–Aldrich* and used without further purification. The purity of chemicals are as follows - tungsten(VI) oxide ≥ 99.8%, ammonium metatungstate hydrate 99%, butyraldehyde 99%, ethanol 99.5%, *n*-dodecane 99%, toluene 99.8%, methylcyclohexane 99%. Fumed silica *Aerosil 200* was supplied by *Evonik.* Gases were bought from *Westfalen* Germany with a purity ≥99.999% (Ar, H_2) or ≥99.5% (CH_4) or from Airgas USA LLC classified as ultrahigh purity (H_2, Ar), research grade (CH_4), or grade 5.0 (CO). Argon was used as the inert gas in all experiments unless mentioned otherwise.

2.2. Silica-stabilized tungsten oxide

Silica (Aerosil 200, pyrogenic silica) was agglomerated, sieved to a particle size of 100 – 300 µm, dried at 200 °C for 1 h and calcined at 700 °C for 8 h. The agglomerated silica particles (BET surface area 217 m^2/g) were loaded with 30 mol-% (49.4 wt.-%) tungsten in an incipient wetness impregnation method using a 0.55 M aqueous solution of ammonium metatungstate. This material was dried for 2 h at 60 °C, for 6 h at 110 °C and calcined at 450 °C for 6 h.

2.3. Tungsten carbide synthesis

Catalyst syntheses were performed in two different apparatus and with varying protocols. The apparatus used to optimize conditions via DOE and produce the samples for butyraldehyde hydrogenation was a horizontal tube furnace. Between 0.6 and 1.4 g of tungsten(VI) oxide precursor, either bulk or silica modified and thus corresponding to between 2.59 and 3.88 mmol tungsten, was loaded in a ceramic boat and placed in the isothermal zone of the furnace. In the temperature-programmed synthesis the sample was heated under reactive gas (20 % CH_4 in H_2, with a velocity of the gas stream of 24.11 mm/s) whereas in the isothermal synthesis it was heated under an inert gas flow before switching to reactive gas at the final synthesis temperature. The exhaust gas stream was monitored using a *ThermoStar* mass spectrometer by *Pfeiffer Vacuum*. The reduction was determined to be complete once the CO concentration dropped close to its original value. In some cases, the reaction was allowed to continue for additional 25% of this reduction time. Afterwards, the catalyst was treated at synthesis temperature with pure H_2 to

remove any excess polymeric carbon from its surface. The material was then cooled down under inert atmosphere and transferred to a glove box.

A fractional factorial 2^{5-1} design with the gas flow inserted as E=ABCD was used. These samples are referred to as “DOE Set” in this paper. The factors and their levels are listed in Table 1, the complete experimental plan is listed in Table S1. An additional center point to confirm linearity inside the parameter range was performed for the silica-stabilized precursor. The response factors were the reduction time, measured by CO evolution during the synthesis; BET surface area and pore volume; W, W_2C and WC content in the catalyst and 1-butanol formation rate as indication of catalytic activity. Evaluation of the experimental results was done in *Design Expert 9* by *Stat-Ease*.

Table 1: Factors investigated in the DOE with their respective levels

Factor	**low level**	**high level**	**center point**	
Synthesis temperature (°C)	700	750	725	A
Prolonged synthesis time (%)	0	25	12.5	B
Amount of tungsten(VI) oxide (mmol)	2.59	3.88	3.24	C
Silica stabilizer	No	Yes	Yes	D
Gas flow rate reactive gas (mL/min)	100	200	150	E=ABCD

After obtaining the results from DOE, a set of four conditions was chosen, and additional syntheses were carried out in a vertical stainless-steel reactor (SS 316) with an outer diameter of 0.25 in and an inner diameter of 0.18 in, heated by a tubular furnace. These materials were made from the same precursors as those of the DOE Set, but the scale of the synthesis was one order of magnitude smaller, and the synthesis time was fixed. These carbides are identified as “Set II”. Between 30 and 50 mg of precursor material was held in place by quartz wool and a 0.125 in stainless-steel support tube, and the temperature was adjusted with an Omega CN-444 controller connected to a thermocouple on the inside of the furnace wall. The reactor was heated to the desired temperature, 700 °C or 750 °C, at a rate of 10 K/min while the sample was in a flow of argon (70 ml/min). At synthesis temperature, the flow was switched to 38 ml/min flow of a 1:4 mixture of methane and H_2. After a synthesis time of 28 min, first methane was switched off, 2 min later H_2 was switched off, and then the sample was cooled in an argon flow. The effluent gas was analyzed by a Pfeiffer Vacuum OmniStar GSD 320 mass spectrometer, and amounts of carbon monoxide and water formed were quantified with the help of calibrations. The obtained carbides were further analyzed by CO adsorption or tested for toluene hydrogenation activity in the same reactor, that is, without exposure to the ambient.

2.4. Catalyst characterization

Tungsten and tungsten carbide crystal phase ratios of samples from DOE conditions were examined using an *Empyrean* X-ray diffractometer by *Malvern Panalytical* operating with Cu Kα radiation. Samples were measured after passivation in air in reflection geometry in the range from 5 – 70 °2θ. Whole-powder-pattern-fitting was performed using the software *HighScore Plus* by *PANalytical*, including a background correction. More details are listed in the supporting information. X-ray diffraction measurements of the four materials synthesized for toluene hydrogenation were performed with a Rigaku Smartlab SE X-ray Diffraction System equipped with a Cu Kα anode X-ray source. The samples were measured in Bragg Brentano geometry with a scanning rate of 2 °/min and a step size of 0.02°. A zero-background sample holder was used to mount the sample. Whole powder pattern fitting was employed to fit the measured diffractograms using PowderCell software. Crystallite size analysis was performed using the Williamson-Hall method analysis provided in PowderCell.

Optical microscopy was done on a digital microscope VHX-500 by Keyence. The microscope was equipped with a digital auto focus and automatic real time depth composition. Images were taken with illumination from above the sample (top light).

Scanning electron microscopy of selected samples was performed with a FEI Magellan 400 XHR instrument that was equipped with a field emission gun and operated at an electron energy of 5 kV.

Surface area and pore volume were determined using a *Quantachrome NovaTouch LX*^{4} with N_2 at -196 °C. BET method was used for the surface area and BJH for the pore volume. The samples were degassed in vacuo at 350 °C for 4 h. Used gases were He (99.999 %) and N_2 (99.999 %).

CO pulse chemisorption on the DOE samples was measured in a setup equipped with an *OmniStar GSD 301 O* mass spectrometer by *Pfeiffer Vacuum*. The setup is described in detail in a previous publication [52]. The used gases were He (99.9999 %), H_2 (99.9999 %) and 1.00 % CO (99.0 %) in He (99.996 %) from *Westfalen* Germany. Samples corresponding to 0.3 mmol W were transferred to the test reactor under exclusion of air. The samples were treated at 350 °C with hydrogen for 120 min and helium for 60 min before measurement. The sample loop volume corresponded to 0.388 µmol CO. Alternatively, CO chemisorption was conducted immediately after synthesis in the stainless-steel reactor. The adsorption temperature was 30 °C or 40 °C, and the pulsed amount was 0.263 µmol CO.

Raman spectra were measured on an *inVia Reflex Raman System* by *Renishaw*, combined with an optical light microscope *Leica DM2700M* (Magnification ×5, ×20, ×50) from *Leica Microsysteme Vertrieb GmbH*. The laser was a 532 nm laser RL532C with an intensity setting of 0.3 mW on the sample. Samples were packed and sealed under argon atmosphere in glass capillaries with a wall thickness of 0.01 mm and an inner diameter of 0.5 mm provided by *WJM-Glas*.

2.5. Catalytic tests

Catalytic butyraldehyde hydrogenations were performed in a 300 mL *Parr* mini reactor. An excess of reactant was used to produce a constant product formation rate over the first few hours. The reaction mixture consisted of 10 mL butyraldehyde, 100 mL ethanol and 1.5 mL of the internal standard *n*-dodecane. The reaction mixture was flushed with Ar before inert addition of 0.25 g catalyst (aldehyde-to-tungsten molar ratio for bulk catalysts of 84 and for SiO_2-stabilized catalysts of 143). The reactor was closed and pressurized with H_2 to 65 bar. The reactor was heated to 200 °C before stirring was turned on. Intermediate sampling of the liquid phase through a dip tube was performed at the start of the reaction and after 15, 30, 45, 60, 90, 120, 180 and 240 min (Figure S1). The catalytic activity was determined by the increase of 1-butanol concentration in samples from 15 min to 180 min, and results were normalized to the amount of tungsten in the reactor. Samples were analyzed using an *Agilent 6980* gas chromatograph from *Hewlett Packard* equipped with an automated injector and FID. Samples were analyzed over a HP-1 MS column with the following temperature-program - holding at 50 °C for 3 min, heating to 140 °C with 20 K/min and further heating to 270 °C with 30 K/min. Retention times and response factors relative to the internal standard were determined using pure substances.

Toluene hydrogenation was conducted in the stainless-steel reactor described in Section 2.3 at a reaction temperature of 250 °C. Liquid toluene was fed to the reactor by a Legato 011 SS continuous injection syringe pump at a rate of 0.15 ml liquid/h. The reactor was pressurized with H_2 to 20 bar gauge for the catalytic test reaction, and H_2 flow was maintained at 75 ml/min (STP), corresponding to H_2:toluene molar ratio of 142:1. The reaction products were analyzed with a Varian CP3800 gas chromatograph, equipped with a CP-Silica PLOT column of 60 m length and a flame ionization detector. Retention times and response factors were determined by calibration with pure compounds. The sole product of toluene conversion at a reaction temperature of 250 °C was methylcyclohexane. Conversions varied between 37 and 95% and cannot be considered to be differential. However, specific rates were invariant to toluene conversion, consistent with a zero-order reaction, as has been found for toluene hydrogenation on noble metals and on molybdenum carbide [50,53]. Carbon balances mostly closed within ±10% and did not exceed

±15% mismatch. Reported rates are averages from the period of 1 to 3 h on stream, when the catalyst performance was nearly stable.

3. Results and Discussion

3.1. Comparison of temperature-programmed and isothermal tungsten carbide synthesis

3.1.1. Principal carburization process

Tungsten carbide synthesis by carburization of a high-oxidation-state precursor proceeds over several reduction and carbon insertion steps. The typically observed products for this process include bulk solid phases W, W_2C, and WC and volatile products H_2O and CO, as illustrated in Scheme 1. In addition, carbon may be deposited on the solids. It is important to note that reduction is connected to CO and H_2O formation while carbide formation is not unambiguously tied to gas phase products even though the hydrogen atoms from methane must evolve in some form. The observation of CO however is an indicator of a surface capable of activating methane, and has previously been linked to carburization [54].

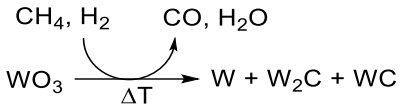

Scheme 1: Conversion of tungsten trioxide to metallic tungsten and tungsten carbides through reaction with a CH_4/H_2-mixture. Carbon monoxide and water are volatile products of the reaction.

To steer this process and obtain the desired phase, the relative rates of reduction, carbon source activation and carbon incorporation must be correctly balanced and excess carbon deposition must be avoided. The parameter space is immense, and we start here by highlighting the differences between a typical classical temperature-programmed synthesis of tungsten carbide and an isothermal synthesis. The structural and catalytic properties of the obtained materials indicate that the isothermal synthesis has merit and deserves further investigation, as does the addition of silica as stabilizer.

The transformation of the precursor to the tungsten carbide catalyst proceeds differently for temperature-programmed synthesis (TPS) and for isothermal synthesis, as can be seen in Figure 1. In the TPS, the tungsten oxide precursor is heated in the reactive gas mixture (20% CH_4 in H_2) from RT to the synthesis temperature of 700 °C. During this heating process, two water release events are detected in the effluent gas stream, suggesting extensive reduction prior to activation

of the carbon source. The onset of the first is at 350 °C and the second starts at 500 °C. The CO formation only begins shortly before the final synthesis temperature is reached and the reduction proceeds at 700 °C.

In the isothermal synthesis, the precursor is heated under inert gas and only exposed to the reactive gas after reaching the synthesis temperature. Contact to the reactive gas immediately leads to the formation of water, while CO is only detected after an initiation period. In comparison to TPS, a longer holding time at the synthesis temperature of 700 °C is needed before H_2O and CO evolution cease and the reduction-carburization process can be considered complete.

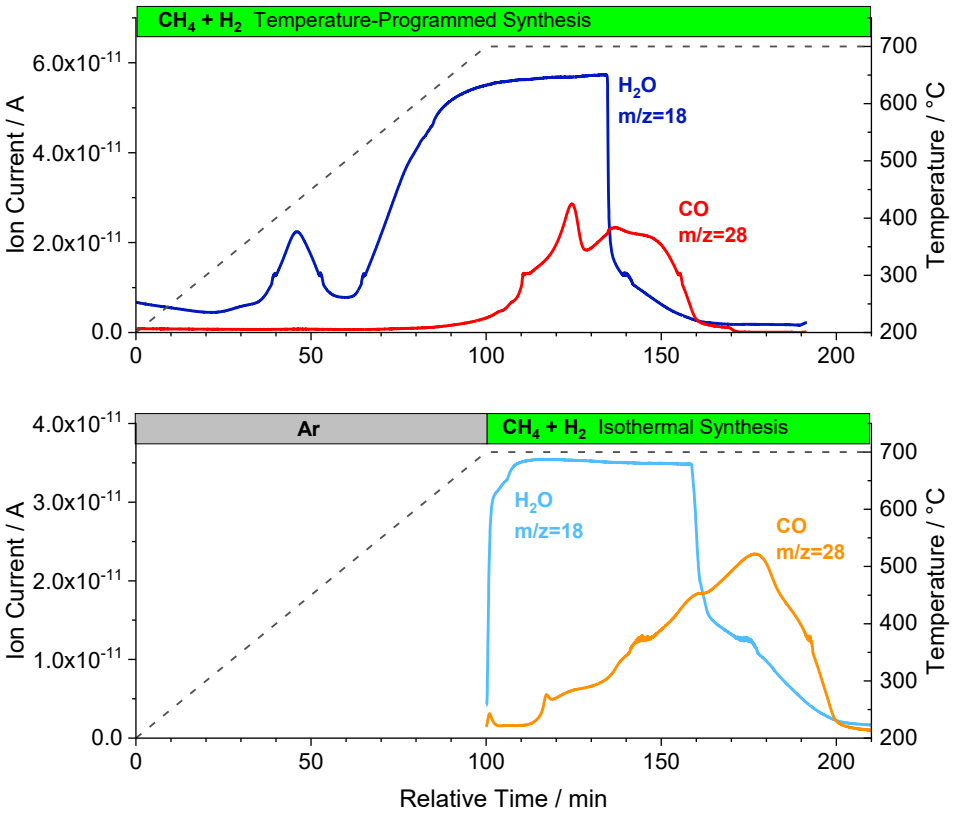

Figure 1: Comparison of gas evolution during tungsten carbide synthesis. Top, temperature-programmed synthesis with reactive gas mixture CH_4 + H_2 present from beginning of heating ramp; bottom, isothermal synthesis, reactive gas mixture CH_4 + H_2 introduced upon reaching the holding temperature. Shown are the MS traces of the main products, H_2O (m/z=18) and CO (m/z=28). Silica-stabilized tungsten oxide precursor, heating rate 5 K/min, holding temperature 700 °C.

3.1.2. Synthesis method and phase composition

The carbide catalysts obtained at the synthesis conditions in Figure 1 are composed of a mixture of metallic tungsten, tungsten semicarbide (W_2C) and tungsten monocarbide (WC). The TPS results in a mixture of all three phases with a preference to W_2C and metallic tungsten. The

isothermal synthesis on the other hand results in mostly W_2C with only a small amount of W, while little WC can be detected. Both diffractograms are depicted in Figure 2. Preventing the pre-reduction improves the phase purity and favors W_2C formation. The addition of silica further increases the W_2C content and reduces the metal content.

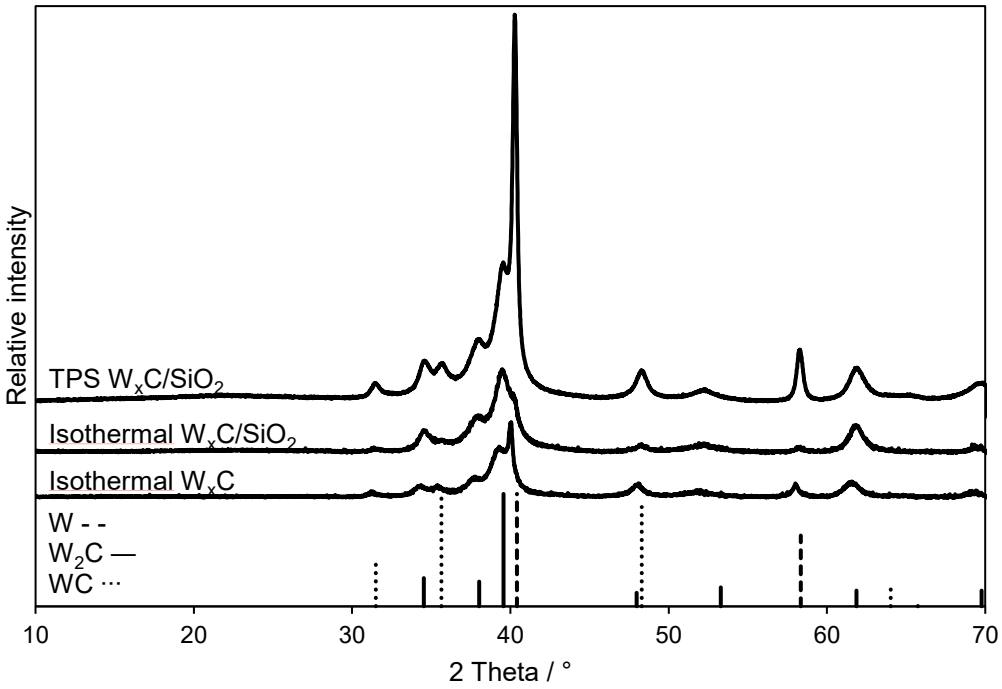

Figure 2: X-ray diffractograms of tungsten carbide catalysts. Two silica-stabilized catalysts, prepared in a temperature-programmed synthesis (blue) and under isothermal conditions at 700 °C (orange, DOE-15) and one bulk catalyst prepared under isothermal conditions at 700 °C (green, DOE-7). Data shifted along y-axis. The exact phase composition is determined by whole-powder-pattern-fitting (supporting information). Reference patterns from ICDD database (W: 00-001-1203, W_2C: 00-035-0776, WC: 01-089-2727) [55–57].

3.1.3. Effect of synthesis method on catalytic activity

The W_xC-catalysts, prepared according to the two different routes, are active for catalytic hydrogenation of butyraldehyde, in a liquid-phase batch process. Over the first 180 min of reaction time, the hydrogenation proceeds with a constant rate of formation of the reaction product 1-butanol as shown in Figure 3. The selectivity towards 1-butanol is approx. 80 % for all catalysts, with deoxygenation as the major side reaction resulting in the formation of butane and butene [12]. The alkane and alkene are gaseous at standard pressure and room temperature and can therefore not be quantified in the liquid aliquot. An exemplary reaction progress including reactant and product concentration is depicted in Figure S1.

The isothermal carbide synthesis results in a catalyst with a more than two-fold increase of the 1-butanol formation rate per mol tungsten from 12.00 h^{-1} to 26.31 h^{-1}. The cause of this increase in catalytic activity, which might be the result of more active sites or a larger number of sites, will be elucidated in Section 3.4. The isothermal carbide synthesis prevents pre-reduction and results in more active hydrogenation catalysts. To optimize this method, the importance of different synthesis parameters will be established in the next section by using design of experiments.

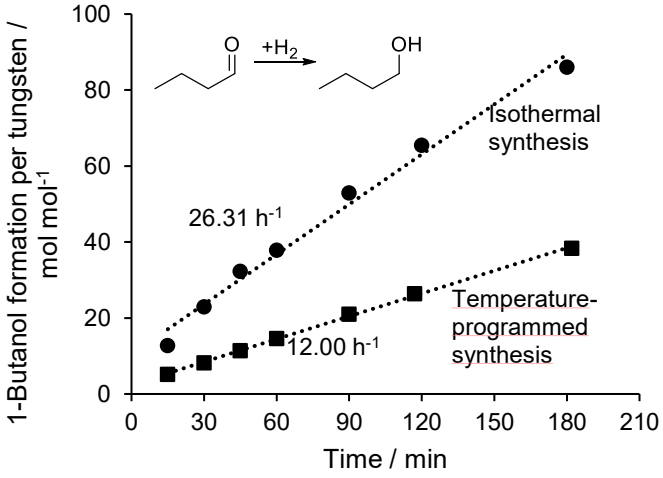

Figure 3: 1-Butanol formation normalized to the tungsten content for a silica-stabilized tungsten carbide catalyst prepared in a temperature-programmed synthesis (squares) or under isothermal conditions at 700 °C (circles). Catalytic tests are performed at 200 °C, 65 bar H_2-pressure and ethanol as solvent with 0.25 g of catalyst and 8.10 g of butyraldehyde, corresponding to an aldehyde-to-tungsten molar ratio of 143.

3.2. Synthesis parameter investigation in a Design of Experiments approach

3.2.1. Rationale for variable and constant synthesis parameters

In a design of experiments (DOE) approach, parameters (factors) are varied in a specific way that allows conclusions to be drawn regarding their importance and interactions, while at the same time verifying the statistical significance of the findings [49]. DOE has not been applied to carbide synthesis before, and establishing which synthesis parameters have a significant influence on the carbide formation and on the produced catalyst is valuable in understanding and optimizing the isothermal carbide synthesis. At the same time, understanding which parameters do not play a significant role is just as valuable. Based on literature, preliminary results, and some additional considerations, we select the synthesis parameters to be varied within the DOE approach and those to be kept constant.

The presence or absence of a silica stabilizer is one variable of interest, based on the literature mentioned in the introduction and the XRD results in Figure 2. The tungsten content in stabilized materials was held constant at 30 mol%. Solid-state diffusion is a rate-limiting process during the synthesis, making temperature an obvious variable; in turn, precursor particle size was not varied. The partial pressure of methane was kept constant, corresponding to a concentration of 20% at atmospheric pressure. Assessing completion of the synthesis while preventing carbon deposition is difficult without in situ product characterization. A first assumption would be that carbide synthesis is completed once the reduction is finished and the CO concentration in the effluent gas stream returns to its original value. Using this dynamic method to determine the synthesis time ensures that the reduction of the tungsten(VI) precursor is complete while at the same time exposure to the reactive gas is limited and over-carburization and excessive coke formation is prevented. However, to verify the underlying assumption of a complete carburization, a 25% extended synthesis time was included in the parameter space. We also varied the space velocity to test whether the results are confounded by heat and external transport limitations.

The experimental plan is a fractional factorial 2^{5-1} design with the reactive gas flow rate inserted as the product of the other four parameters. This insertion of the additional parameter cuts the number of experiments needed from 32 to 16 with only minimal loss of information. The experimental plan and the corresponding analyses are listed in Tables S1-S3 of the supporting information.

The response factors and their values are given in Table 2. Figure 4 compiles the importance of relevant parameters on the respective response factor, normalized to the most influential parameter, for all cases where more than one parameter is relevant. The chance for any of these results to occur randomly is only 0.01%.

The reduction time is primarily dependent on temperature and gas flow, whereas both W_2C content and catalytic activity are strongly influenced by synthesis temperature and the presence or absence of silica stabilizer.

Table 2: Crystalline phase composition with goodness of fit for the whole-powder-pattern-fitting, 1-butanol formation rate normalized on amount of tungsten in catalysis test, BET surface area and pore volume for isothermal carbide synthesis (DOE Set of samples)

Entry*	Synth. temp. (°C)	Synth. Time* (%)	n(WO_3) mmol	Stabilizer -	Reduction time (min)	W (wt.-%)	W_2C (wt.-%)	WC (wt.-%)	Goodness of fit -	1-Butanol formation rate (h^{-1})	BET surface area (m^2/g)	Pore volume (cm^3/g)
1	700	0	2.59	Bulk	78	29.5	65.7	4.8	1.20	19.27	16.84	0.031
2	750	0	2.59	Bulk	70	5.7	15.3	79.0	2.04	5.61	22.42	0.053
3	700	25	2.59	Bulk	110	21.0	22.4	56.6	1.63	8.13	14.53	0.042
4	750	25	2.59	Bulk	39	9.1	13.5	77.4	1.82	6.07	19.28	0.058
5	700	0	3.88	Bulk	152	18.1	40.5	41.4	1.17	9.52	21.57	0.058
6	750	0	3.88	Bulk	62	7.8	14.5	77.7	8.23	6.07	20.97	0.061
7	700	25	3.88	Bulk	82	17.0	70.0	13.0	1.38	15.59	22.24	0.047
8	750	25	3.88	Bulk	86	4.5	13.9	81.6	2.48	5.43	14.05	0.041
9	700	0	2.59	SiO_2	107	21.7	74.3	4.0	1.43	20.91	110.27	0.585
10	750	0	2.59	SiO_2	36	21.6	54.2	24.1	1.36	16.30	60.75	0.375
11	700	25	2.59	SiO_2	60	20.3	79.1	0.7	1.57	22.55	93.87	0.562
12	750	25	2.59	SiO_2	56	2.8	48.6	48.6	1.84	19.09	102.73	0.622
13	700	0	3.88	SiO_2	80	25.7	74.0	0.2	1.63	23.60	90.85	0.480
14	750	0	3.88	SiO_2	76	5.0	63.7	31.3	1.55	19.07	73.09	0.441
15	700	25	3.88	SiO_2	134	4.3	91.9	3.8	2.78	26.31	96.84	0.517
16	750	25	3.88	SiO_2	48	6.7	51.5	41.8	1.29	17.98	85.23	0.494
Central point	725	12.5	3.24	SiO_2	65	15.5	65.1	19.5	1.63	19.38	-	-
Extrapolation 775 °C	775	25	2.59	SiO_2	26	10.0	37.5	52.5	1.46	13.25	-	-
Extrapolation 680 °C	680	50	3.88	SiO_2	160	5.4	94.3	0.3	3.34	26.19	-	-
Extrapolation 670 °C	670	0	2.59	SiO_2	144	26.7	73.3	0.0	11.02	20.11	-	-

**Exps. 1-8, WO_3 only, all other WO_3 with SiO_2.*

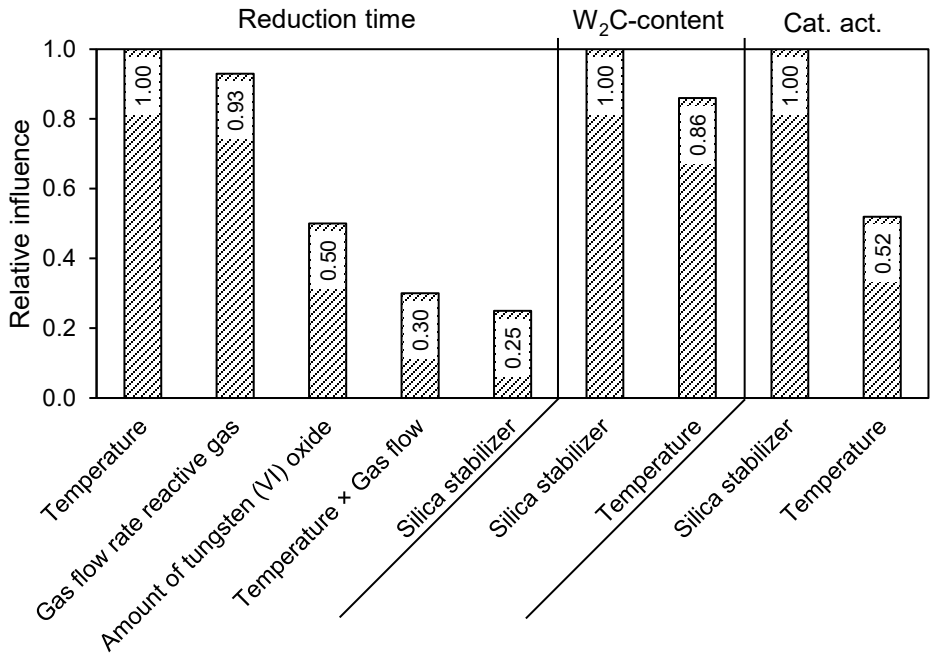

Figure 4: Relative influence of significant parameters and their interactions on reduction time, W_2C-content and catalytic activity in the 1-butanol formation according to results from the DOE.

3.2.2. Reduction time and fate of oxygen

The concentrations of H_2O and CO in the effluent gas stream during the isothermal carbide synthesis are depicted exemplarily in Figure 1. Once the CO-concentration declines to its initial value, the reduction is assumed complete. The time until complete reduction is, in decreasing order of impact, dependent on the synthesis temperature, the gas flow rate, the amount of WO_3 in the reactor, an interaction of gas flow rate with the temperature, and the presence of the silica stabilizer (Figure 4). Prolonging the synthesis time past the reduction time obviously does not have an influence on the reduction time itself.

The different synthesis parameters influence the reduction time as would be expected: A higher synthesis temperature and higher gas flow rate decrease the time needed, while using more WO_3 increases it. The influence of the synthesis temperature is more pronounced at low gas flow rates and less influential at high gas flow rates. This trend indicates that mass transfer plays a role. The silica support slightly accelerates the reduction, likely because of a smaller precursor crystallite size or a better accessibility of the tungsten oxide in the dilution medium.

We quantified the amount of CO and H_2O formed for a subset of four isothermal syntheses and found little influence of the synthesis temperature (700 °C or 750 °C) and the nature of the

precursor (with or without SiO_2). Roughly 80% of the oxygen in WO_3 was removed in the form of water, and about 20% in the form of carbon monoxide.

3.2.3. Phase composition

The isothermal carbide synthesis can result in the formation of the crystalline phases metallic tungsten, W_2C, and WC, depending on synthesis conditions. The mass ratios of the two tungsten carbide phases as determined by XRD are dependent on the synthesis temperature and the use of the silica stabilizer. Catalysts prepared at 700 °C show more W_2C, whereas the higher synthesis temperature of 750 °C results in more WC. Example X-ray diffractograms are depicted in Figure 2, including one of a bulk and one of a silica-stabilized catalyst. Results for the crystalline phase composition are determined by whole-powder-pattern-fitting and are listed in Table 2. The entire set of diffractograms from the DOE approach is shown in Figure S2, together with information on the data treatment.

The patterns used for fitting were ICDD #00-001-1203 for W, #00-035-0776 for W_2C, and #01-089-2727 for WC. The IUPAC notation of the W_2C is (*hP3*, *P$\bar{3}$m1*) (CdI_2 type), it is alternatively known as β‘‘-W_2C or α-W_2C. We note here that the measured diffractograms are consistent with this structure, but not conclusive. A distinction of the four different polymorphs of W_2C by powder XRD is nearly impossible, because the tungsten sublattice is the same in all variants and the X-ray scattering factor of carbon is small [27,58]. The other options are β-W_2C (L‘3 Type, *P6$_3$/mmc,* ICDD #01-077-8464), β‘-W_2C (ζ-Fe_2N-Type, *Pbcn,* ICDD #00-020-1315), and ε-W_2C (ε-Fe_2N-Type, *P$\bar{3}$1m,* ICDD #01-076-7103). The diffractograms would only be distinguishable by reflections of low intensity at low angles [58], and these were not detectable. The stick patterns of these four phases (generated from the ICDD cards) are shown in Figure S3 to illustrate their similarity. The IUPAC notation of the used WC is (*hP*2, *P$\bar{6}$m2*) (WC type); it is also known as δ-WC.

The silica stabilizer drastically increases the amount of W_2C, which reaches up to 91.9 wt.-%. In contrast, the highest W_2C-content that could be reached in the absence of silica was 70 %. This strong stabilizing effect is especially remarkable considering the high tungsten-metal loading of 49.4 wt.-% in the precursor. Usually, in the tungsten carbide synthesis with a gaseous carbon source the carbon insertion is difficult to control, and the fast carburization preferentially results in the formation of the thermodynamically favored WC.

The other synthesis parameters do not change the ratio of tungsten carbides in a significant manner. Interestingly, prolonging the carburization time by 25% of the reduction time does not noticeably increase the carbon insertion into the tungsten metal, that is, the fraction of WC did not

increase. It appears that the carbon insertion proceeds substantially slower once the reduction is completed.

3.2.4. Catalytic activity

The catalytic activity, defined as the product formation rate per tungsten (in moles alcohol per mol W per time), for isothermally synthesized catalysts is only dependent on the synthesis temperature and the presence of the silica stabilizer (Figure 4). A lower synthesis temperature increases the catalytic activity, as does the presence of the silica stabilizer. Gas flow rate, amount of WO_3 in the synthesis reactor and prolonging the synthesis time do not change the catalytic activity, at least not in the investigated parameter range and if complete reduction is guaranteed.

The isothermal synthesis together with the control of the reaction time decouple the catalytic activity from several synthesis parameters. The gas flow rate influences the time until complete reduction is reached but does not alter the catalytic performance. Therefore, this parameter can be set to suit different synthesis setups. Similarly, using more tungsten oxide increases the time needed for the synthesis, but the inherent properties of the final catalyst remain the same. With this information, a limited up- or down-scaling can be implemented quite easily, adapting the amount of prepared catalyst to fit different needs.

3.2.5. Catalyst optimization by extrapolation of the DOE

The results of the DOE allow the prediction of catalytic activity or W_2C-content dependent on synthesis temperature and use of the silica stabilizer. The W_2C-content and the activity of the catalysts behave concurrently, which will be analyzed in more detail in Section 3.4. This linear model for the synthesis of W_xC-catalysts is at first only valid for the originally investigated temperature range from 700 °C to 750 °C. A central point synthesized at 725 °C fits the value predicted by the model and confirms its linearity in this range. It is possible to extrapolate the model outside of the original temperature range to help optimize the catalyst synthesis, although care has to be taken in choosing suitable conditions. Figure 5 depicts the results of this extrapolation for the silica-stabilized system. Moving to a higher W_xC synthesis temperature of 775 °C is predicted to result in less W_2C and a diminished catalytic activity, whereas performing the synthesis at a lower temperature of 680 °C should yield a catalyst with more W_2C and a higher catalytic activity. Both predictions are confirmed experimentally with an exceptionally high agreement between experimental and predicted values (Figure 5, diffractograms in Figure S4). At an even lower synthesis temperature of 670 °C the linear model predicts 100 % W_2C and accordingly the highest possible catalytic activity, but experiments show a drop in catalytic activity. As can be expected for a linear model its predictive capabilities break down when it is approaching

its natural boundaries. At such a low synthesis temperature, the carbon insertion does not proceed sufficiently, more metallic W and less W_2C is produced, resulting in a less active catalyst. Nevertheless, using a DOE approach together with catalyst characterization allows optimizing the catalytic performance of the tungsten carbide/silica system in a very efficient and goal-oriented manner.

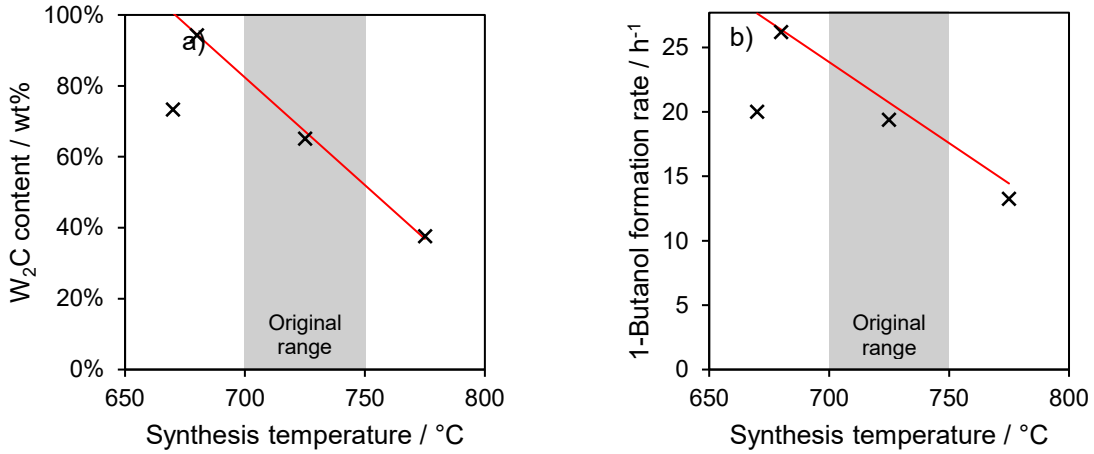

Figure 5: Predicted (line) and experimental (×) values for a) W_2C-content and b) 1-butanol formation rate for silica-modified catalysts at different synthesis temperatures.

3.3. Relationship between phase composition and particle size

3.3.1. Hypothesis of relationship between particle size and phase stability

The data in the preceding section indicate a mixture of W_2C, WC, and some W, depending on synthesis conditions. There are several reasons as to why W_2C could be observed; kinetics could allow it to exist as metastable phase, but there are also factors that could render W_2C thermodynamically more favorable than WC. The carburization process from oxide precursors naturally first results in structures with lower carbon content. Ostwald's rule calls for crystallization of less stable prior to more stable phases. Thermodynamically, carbon chemical potential is important. Further, W_2C could be thermodynamically stabilized if the particles were small enough for the surface energy term to prevail in the overall Gibbs energy of the phase. Literature suggests that W_2C has a surface energy that is 0.5 J/m^2 lower than that of WC [59]. The difference in the free energy of formation for the two tungsten carbide phases is 61.3 J/g [60]. Detailed recent work by Shrestha et al. [33] suggests δ-WC is stable at crystallite sizes > 10 nm while the various polymorphs of W_2C are stable at smaller crystallite sizes. Consequently, crystalline domain size and morphology constitute important information to possibly discriminate these phenomena.

3.3.2. Microscopic analysis of carbide particles

One of the two key synthesis parameters affecting phase composition is the presence or absence of a silica stabilizer. The light microscopy images in Figure 6 show that the commercial tungsten oxide precursor is coarse crystalline with particles of up to 100 µm in size. The macroscopic size and shape of these particles are maintained during the carburization process. In contrast, the silica-stabilized precursor is characterized by the smooth silica particles with a yellow coating, indicative of dispersed WO_3, with the occasional greenish, large WO_3 particle. After carburization, the silica particles are covered with a black material that has a metallic sheen, consistent with the properties of a transition metal carbide.

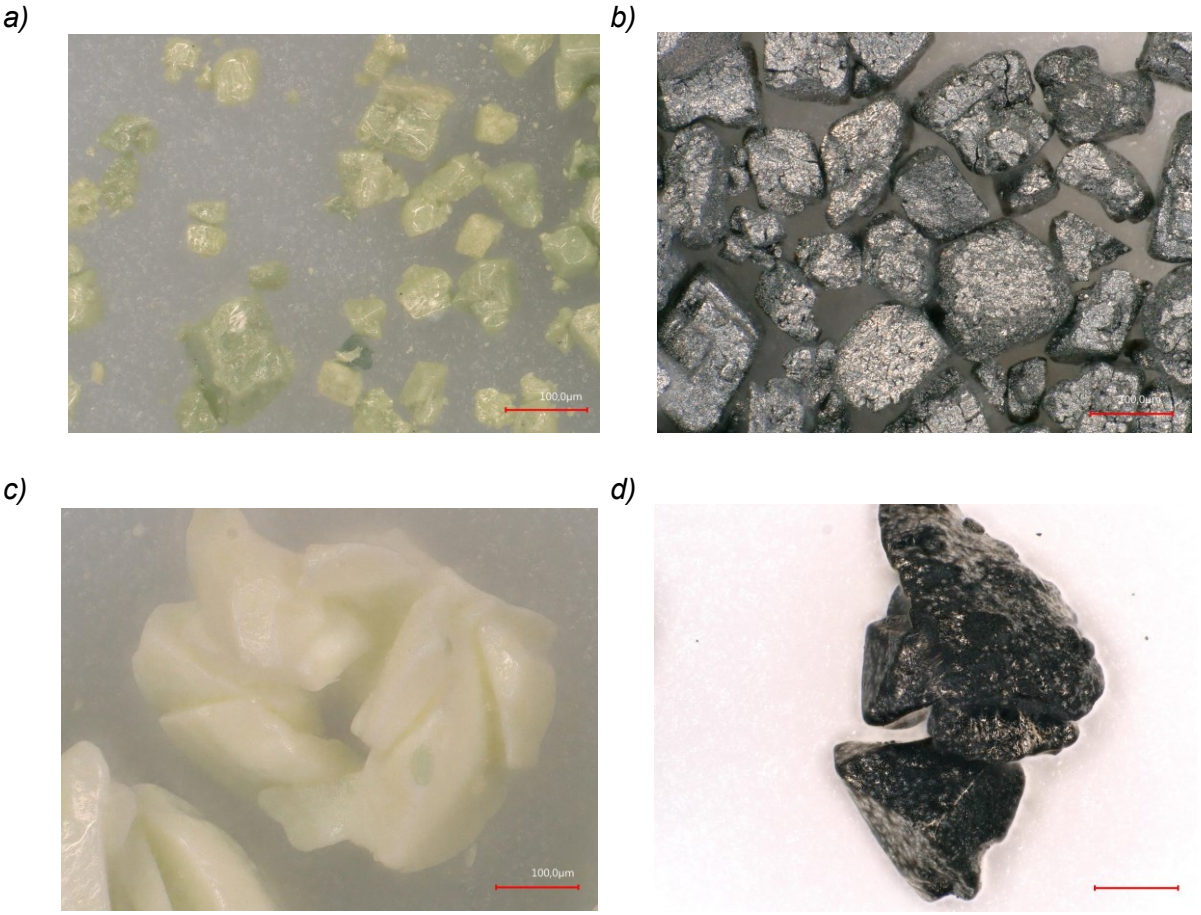

Figure 6: Light microscopic images (magnification ×500) of a) bulk tungsten oxide, b) bulk tungsten carbide, c) oxide–silica precursor and d) silica-stabilized tungsten carbide (27 mol% W). The carbides were prepared in an isothermal synthesis using 3.05 mmol W. The conditions of 100 ml/min flow 20 % CH_4 in H_2 at 700 °C with a synthesis time equal to the reduction time correspond to those of DOE Set Entries 1,5,9,13 in Table 2. The scale bars correspond to 100 µm.

Scanning electron microscopy (SEM) provides a better perception of the transformation of the oxide into a carbide. It is well known that the carburization process enhances the surface area, which for the starting bulk tungsten oxide is usually but a few m^2/g. Moreover, the density of the carbides is more than two times the density of the oxide (17.1 g/cm^3 for W_2C vs. 7.2 g/cm^3 for WO_3), implying a corresponding volume change during the transformation. If the macroscopic dimensions of the oxide particle are retained, then the particle must become porous. Indeed, the image in Figure 7a shows a particle with typical original shape of the oxide but highly porous through subdivision by numerous crevices and tunnels. At larger magnification (Figure 7b), it can be seen that the material is composed of many small crystallites. Since this sample consists almost exclusively of W_2C according to XRD, the crystal habit of this phase is revealed in the images. However, only one half of each of the crystals is recognizable because of tight packing, and these halves appear as pyramids with rhombic faces. Shrestha et al. [33] predicted shapes of different carbide phases (by Wulff construction), and the crystals in the image have the nearest resemblance with the expectations for ε-W_2C. Analysis of a set of four samples (Set II, with and without silica, carburized at 700 °C or 750 °C) by SEM was not conclusive with respect to particle sizes or shapes of the different tungsten phases (W, W_2C, WC), as they could not easily be discriminated in the images for their common metallic nature and difficult-to-measure carbon content.

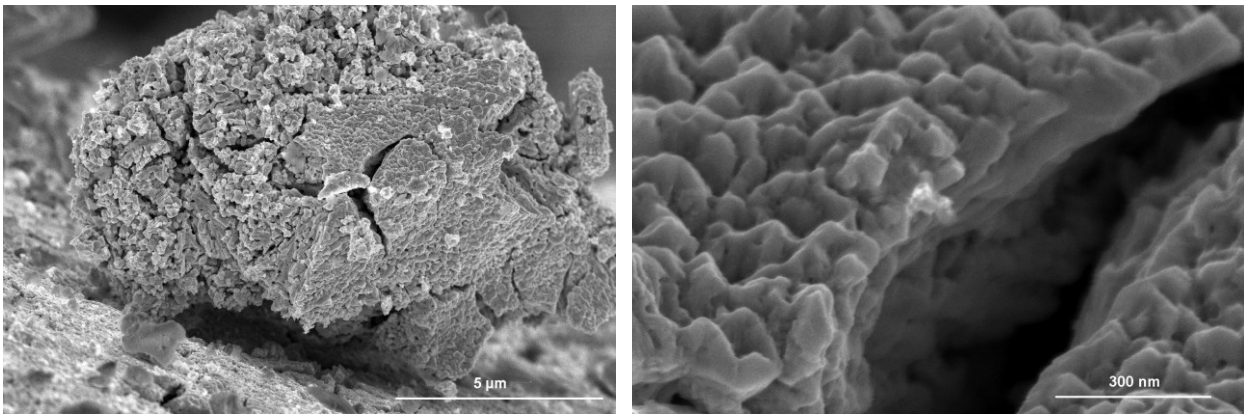

Figure 7: Scanning electron microscopy images of tungsten carbide prepared by isothermal synthesis in a flow of 20 % CH_4 in H_2 at a temperature of 700 °C. Samples from Set II, conditions mirror those of DOE Set Entries 3,4,11,12.

3.3.3. BET surface area and pore volume

Additional, indirect information on the particle size is provided by the N_2 BET surface. For materials without silica, the value is useful as there is no concern about passivation layers as with chemoselective probes. For silica-stabilized materials, there is no distinction between silica area and that of the catalytically active component. The results are listed in Table 2. For bulk W_xC, the surface area is between 14 – 22 m^2/g, and the pore volume is between 0.03 – 0.06 mL/g. An

increase in surface area relative to the WO_3 precursor, for which typically < 5 m^2/ g are measured [47], is expected after carburization to tungsten carbide. Moreover, the sorption data are commensurate with the porous appearance in the electron microscopy images. The silica itself exhibits a surface area of 217 m^2/g and a pore volume of 1.62 mL/g after calcination at 700 °C. Assuming formation of W_2C, the samples contain ~43 wt% SiO_2, implying that the stabilizer could contribute around 93 m^2/g and 0.70 mL/g, unless its properties are affected by sintering or pore blocking. Samples containing the silica stabilizer were characterized by an overall surface area of 60 – 110 m^2/g and a pore volume of 0.38 – 0.62 mL/g. The effect of the silica stabilizer on the tungsten carbide BET surface area is thus not easily extractable. The BET surface area, as well as the pore volume, are found to be only dependent on the presence of the silica stabilizer and do not show any correlation with any other synthesis parameter or with the phase composition.

3.3.4. Analysis of crystalline domain sizes by powder X-ray diffraction

All diffraction patterns were fit, and the crystalline domain sizes of W_2C and WC, as far as they were present in reasonable concentrations, were determined. The resulting values are shown in Figure 8 as a function of synthesis temperature, with the presence or absence of the SiO_2 stabilizer as a parameter. A more detailed version of the plot is shown in Figure S5. It is evident that the crystalline domain size of W_2C is mostly between 7 and 10 nm and therefore smaller than that of WC, which exclusively appears at crystalline domain sizes larger than 10 nm. In other words, each tungsten carbide phase appears within a distinct range of crystalline domain sizes. The stability of δ-WC at crystallite sizes larger than 10 nm is in perfect agreement with the computed phase diagrams by Shrestha et al. [33]. The W_2C phases computationally predicted to be stable in the observed crystallite size range of 6 – 10 nm are the phase with the *Pbcn* space group (termed β-W_2C by Shrestha et al. and β'-W_2C by Kurlov and Gusev) and the phase with the $P\bar{3}1m$ (termed ε-W_2C by Shresta et al. and by Kurlov and Gusev). As stated earlier, the W_2C phases cannot be discriminated by powder XRD, and we can neither confirm nor refute the proposed stability trends among the W_2C phases. The main outcome of the analysis in Figure 8, which is that the W_2C phase is characterized by smaller crystallites than the WC phase, is not affected by this lack of distinction. Higher synthesis temperatures promote a higher fraction of WC, while there is no trend to larger crystallite sizes with increasing synthesis temperature for W_2C; seen together, these trends are consistent with transformation of W_2C into WC upon temperature-induced growth.

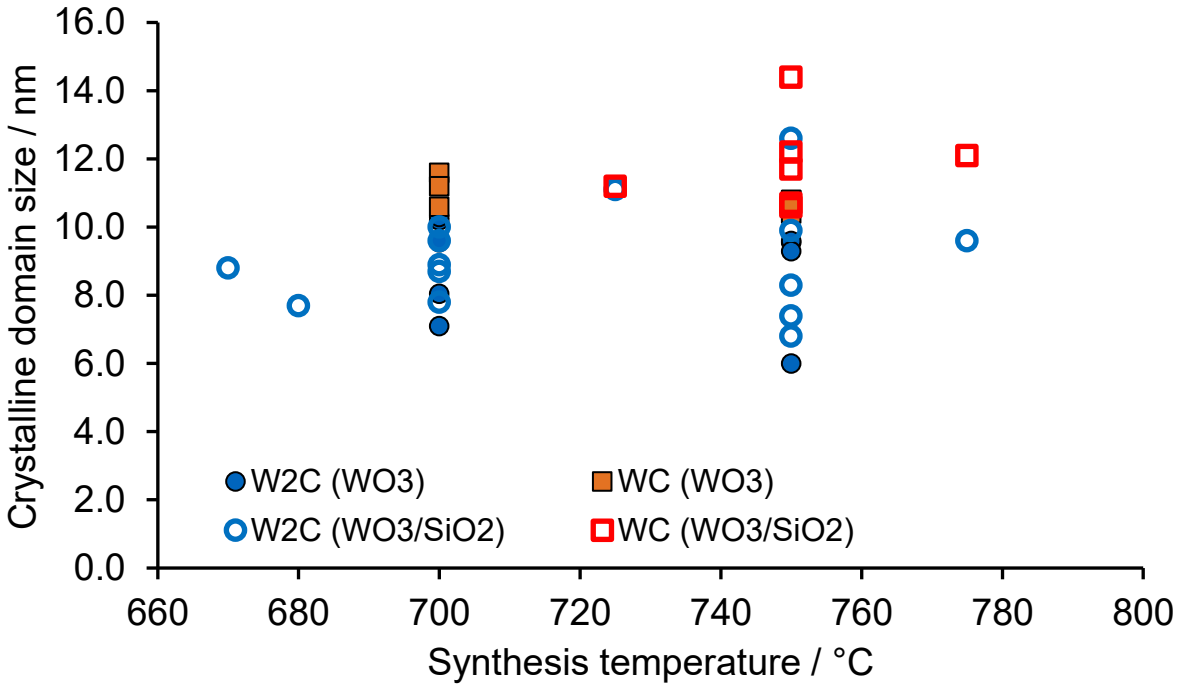

Figure 8: Crystalline domain sizes of W_2C and WC for DOE Set and Set II from powder X-ray diffraction whole pattern fitting. Samples are either made from bulk WO_3 ("WO_3") or from silica-stabilized WO_3 ("WO_3/SiO_2"). Circles, W_2C, squares, WC, open symbols, silica-stabilized, solid symbols, bulk samples.

While the silica stabilizer leads to a higher fraction of W_2C, the observed crystallite size for each phase, W_2C or WC, does not show an obvious correlation with the absence or the presence of the silica stabilizer, as per Figure 8. However, there are two materials containing W_2C crystals larger than 10 nm, and both are silica-stabilized materials. The predictions by Shrestha et al. [33] are based on a vacuum environment, whereas the stabilized carbide particles exhibit both, exposed surfaces that are in contact with the gas atmosphere, and interfaces to the silica. The silica has a high BET surface area and can impart an internal surface area of 161.2 m^2/g on the carbide at a tungsten loading of 30 mol-% (estimate details in SI). While the surface energy of this interface is not known, the contribution could affect the stability ranges and can serve as a possible explanation for larger W_2C particles than would be expected in a vacuum environment. There could be additional interfaces between the tungsten phases.

The silica stabilizer does promote a higher W_2C content (Figure 4), and the reason is evident from Figure 6, which shows that the WO_3 precursor is dispersed on the silica particles, much different from the bulk WO_3 precursor. The dispersion of WO_3 on the silica support is conducive to smaller carbide particles, which are more likely to assume W_2C structure. The interface to the silica could also contribute to stabilization as discussed. The hypothesis posed in the introduction that at small particle sizes, when the surface energy term becomes relevant, the stability order of

different tungsten carbide phases may change, is confirmed. This knowledge opens new possibilities to control carbide phase composition by tailoring carbide crystalline domain size, for example by the precursor crystallite size, the synthesis temperature, or tribochemistry.

3.4. Surface properties and structure-activity relationships

3.4.1. Carbon monoxide adsorption

Carbon monoxide adsorption is commonly used to probe carbide surface area. Here, it was conducted in pulse mode at above ambient temperature, and the results are not confounded by adsorption on the silica stabilizer [36]. Strong and irreversible adsorption is presumably specific to low valence tungsten sites that allow for π back-bonding. The chemisorption followed the synthesis without exposure of the samples to air, thus avoiding passivation from contact with oxygen and the need for re-reduction. The absence of carbon deposits was verified by Raman spectroscopy (Figure S6).

For the silica-free samples, the amount of CO adsorbed per gram is roughly one order of magnitude (*i.e.*, a factor of 7 to 17) lower than the amount of N_2. There is no obvious correlation between the amount of N_2 and the amount of CO for the limited set of samples investigated, suggesting that the surface electronic properties of these polycrystalline, multiphase samples are not uniform and the metallic fraction on which CO adsorbs varies from sample to sample. The amount of CO was found to be linearly correlated to the fraction of W_2C, as demonstrated in Figure 9. This correlation applies to both types of materials, those without and those with silica stabilizer.

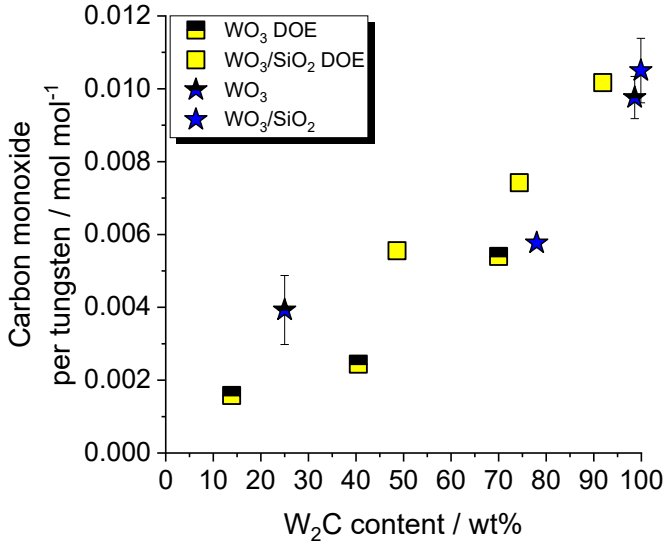

Figure 9: Carbon monoxide adsorption as function of W_2C content, as amount CO adsorbed in moles per mole tungsten in the sample. Two sample sets are shown, with carbide syntheses performed in different reactors and chemisorptions in different apparatus. Yellow squares are from DOE Set, blue stars represent Set II.

The trend in Figure 9 indicates that the main contribution to the metallic surface area comes from W_2C. The crystalline domain size of W_2C is generally smaller than that of WC, and one could hypothesize that the particle size is also smaller and hence the metallic surface area larger. However, a quantitative consideration shows that the difference in domain size is insufficient to explain the difference of one order of magnitude in CO adsorption that becomes apparent from the endpoints in Figure 9. In addition, an estimate shows that spherical crystallites with a 5 nm radius and a density of 17.1 g/cm^3 have a surface area of ≈35 m^2/g, which is significantly higher than the up to 22 m^2/g that are measured. The domain size is thus not a good measure of particle size, and the particles in the W_2C-rich samples consist of smaller crystalline domains. Finally, for the silica-free materials, the N_2 BET surface area is largely invariant to phase composition (Table 2 and Figure S7). Thus, different physical dimensions of the particles of each phase cannot account for the trend in CO adsorption with phase composition.

Since size and morphology cannot explain the difference in CO adsorption, the adsorption properties of WC and W_2C must be different. The literature is controversial with respect to CO adsorption on WC. Initial work by Volpe and Boudart suggested the adsorption is only around 11% of a monolayer [22]; later work by Ribeiro et al. showed a 1 h long treatment in H_2 at a temperature of 700 °C made more sites available for CO adsorption, corresponding to close to 40% of a monolayer [4,20]. The increase in surface area through the H_2 treatment was attributed to the removal of polymeric carbon from the synthesis, which had been conducted at 1100 K. It was reported that some faces of WC do not adsorb CO [4]. Indeed Koverga et al. [61] found that the strongest adsorption is on C-terminated, not on W-terminated faces. From the work of Shrestha et al. [33], WC crystals are more likely to exhibit W-terminated faces than W_2C. Recent application of WC as electrocatalyst revealed that the material is little susceptible to CO poisoning, which was attributed to weak adsorption of the CO molecule [62]. The desorption of CO from WC has been observed to occur largely below 400 K [63]; others reported that on WC(1000), a fraction of CO dissociates and another fraction desorbs below 250 K [64]. Evidently, the surface properties of WC are not firmly established in the literature, which suggests that crystal termination is important. In contrast, the literature is consistent with respect to strong adsorption of CO on W_2C.

The available data and the literature allow a tentative conclusion by elimination of certain scenarios. Polymeric carbon on the surface of the DOE samples was excluded (Figure S6), as was a mere particle size effect (Figure S7). The remaining explanation for the low CO adsorption on WC-rich samples is that the electronic properties of the exposed WC surfaces are not conducive to strong CO adsorption. In contrast, CO adsorbs readily on W_2C.

3.4.2. Catalytic behavior

As already mentioned, the proportion of W_2C in the carbide catalysts and the catalysts' activity for butyraldehyde hydrogenation are influenced in a very similar manner by the same synthesis parameters. The silica stabilizer results in more W_2C and a higher catalytic activity. The same holds true for a lower synthesis temperature. By comparing the W_2C-content to the 1-butanol formation rate normalized to the amount of tungsten used in the catalysis test, as shown in Figure 10a, a clear, linear correlation between the two is established. This correlation indicates that an increased amount of catalytically active sites or more active sites are available in the presence of the W_2C-phase. The amount of WC and the catalytic activity show a negative correlation (Figure S8), which is a natural consequence of the positive correlation with W_2C and the small tungsten metal content. No correlation can be established between the amount of metallic tungsten found in the catalyst and the catalytic activity (Figure S9). A plot of butyraldehyde hydrogenation rate vs N_2 BET surface area shows two clusters of data points, one cluster for bulk materials that shows no correlation, and one cluster for silica-stabilized materials that has a weak trend but a considerable spread (Figure S10).

The catalytic activity for butyraldehyde hydrogenation correlates extremely well with the amount of chemisorbed CO, as is shown in Figure 10b). It should be noted that the reliability of CO chemisorption experiments is dependent on the absolute amount of adsorbed CO, and the values found for the catalysts with little CO adsorption are subject to a comparatively large margin of error. However, the catalytic activity increases in a linear fashion with the amount of adsorbed CO, thus the CO chemisorption experiment perfectly captures the sites for the kinetically relevant step. Consequently, a higher site density makes W_2C a more active catalyst than WC, and not sites that are more active.

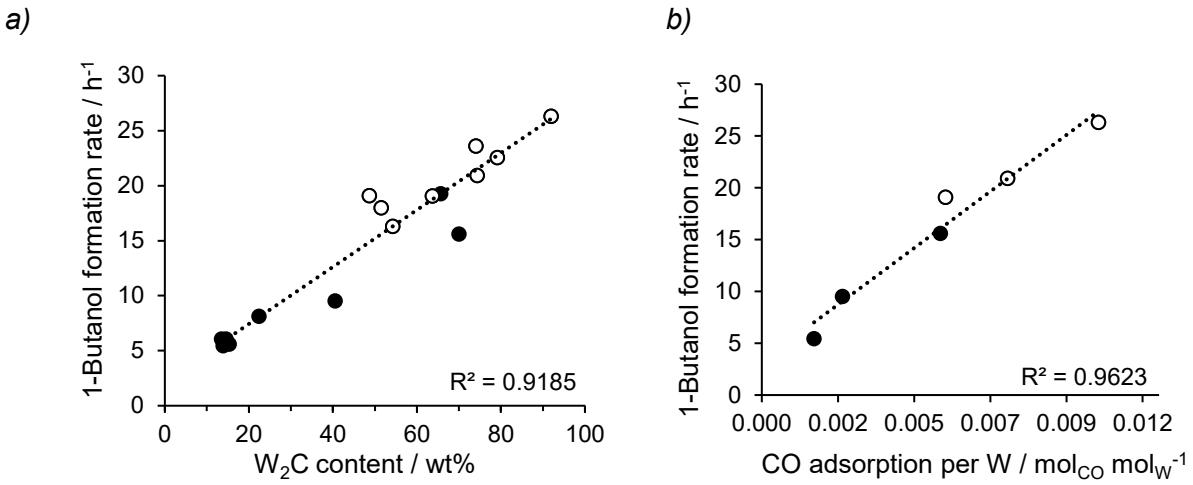

Figure 10: Correlation between the catalytic activity for hydrogenation of butyraldehyde to butanol, expressed as mol 1-butanol per total mol tungsten per hour, as a function of a) W_2C content and b) amount of carbon monoxide adsorbed. Solid circles (●)bulk catalysts; open circles (○)silica-stabilized catalysts.

All samples were active for toluene hydrogenation (Figure S11). The rate of hydrogenation of toluene per amount of tungsten also increases with increasing W_2C content (Figure 11a), although the variation in activity with composition is smaller, and the correlation is not as evidently linear as for butyraldehyde. Similarly, the correlation with the amount of adsorbed CO is less well defined (Figure 11a). The latter is understandable, since ring hydrogenation is reportedly structure-sensitive [50], and CO may not probe the required ensembles adequately. However, individual sites detected by CO are likely part of these ensembles.

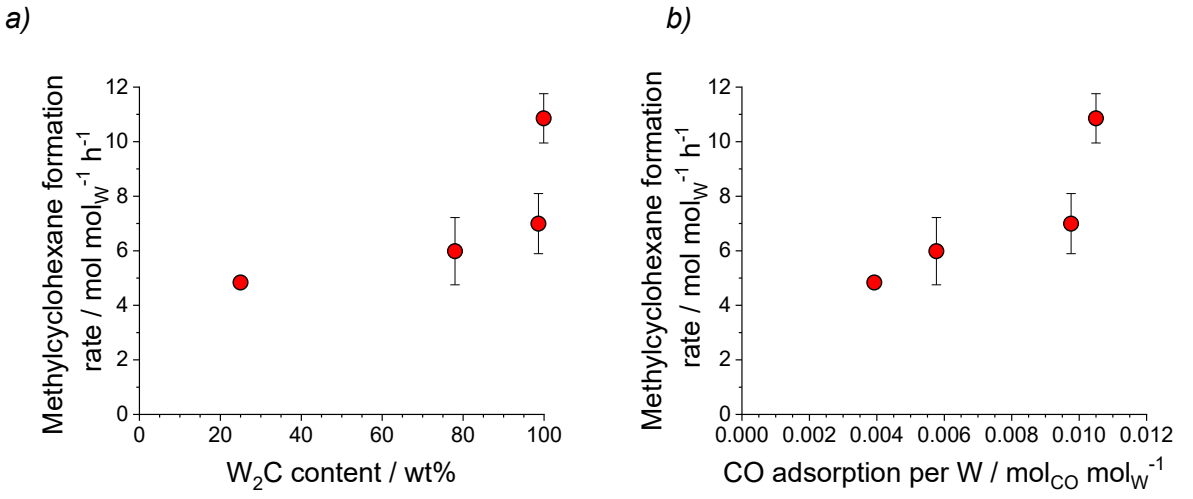

Figure 11: Correlation between catalytic activity for hydrogenation of toluene to methylcyclohexane, expressed as moles methylcyclohexane per mole tungsten per hour, and a) W_2C content and b) amount of carbon monoxide adsorbed.

Combination of Figure 10a with Figure 10b and of Figure 11a with Figure 11b allows generating a correlation of an apparent turnover frequency (TOF) with phase composition, as depicted in Figure 12. The calculation of the TOF is illustrated for butyraldehyde in the supporting information, and the TOFs of the individual catalysts are listed in Table S4. The two plots in Figure 12 indicate that there is little variation of the turnover frequency with phase composition, for both probe reactions. In turn, the total carbide surface area, as probed by CO, is a key factor for activity variations.

There are several possible interpretations of the very similar apparent turnover frequencies that are observed for different phase compositions of the catalysts. One possibility is that W_2C is the only active phase whereas WC does not contribute to the catalytic turnover. Another possibility is that WC does have active sites of comparable activity to those of W_2C, but far fewer as indicated by the low CO adsorption. Prior work indicates that the catalytic transformation dictates which phase is superior. W_2C was found to exhibit a higher turnover frequency in *n*-hexane hydrogenolysis than WC [5], whereas WC excelled in neopentane hydrogenolysis [4]. The observation that butyraldehyde conversion has a more pronounced trend with phase composition than toluene ring hydrogenation is consistent with this notion (Figure 10 vs Figure 11).

Independent from this conclusion, the results indicate the relevance of the complex interplay of synthesis, dispersion (particle sizes), phase composition, chemisorption method and catalytic performance of tungsten carbides for detailed interpretation of structure-activity relationships in catalysis.

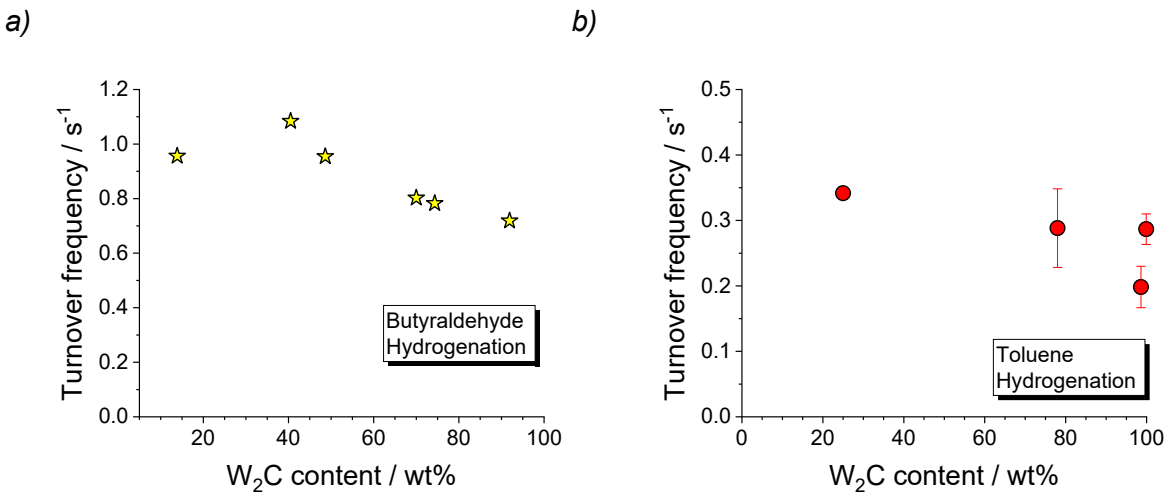

Figure 12: Apparent turnover frequencies, obtained by relating rates to sites as probed by CO chemisorption; a) butyraldehyde hydrogenation to butanol, expressed as mol 1-butanol formed per site per second, and b) toluene hydrogenation to methylcyclohexane, expressed as mol methylcyclohexane formed per site per second. Error bars consider uncertainty in rate measurement from several different syntheses.

4. Conclusions

The isothermal synthesis of tungsten carbides from tungsten oxide precursors with or without silica stabilizer was developed to control the tungsten carbide phase composition. Isothermal synthesis with a dynamic control of the W_xC synthesis time allows complete reduction of WO_3 while preventing over-carburization to WC. A design of experiments approach to optimize the catalyst system was used to efficiently determine the most important synthesis parameters as well as their optimal values. Nearly phase-pure tungsten semicarbide (W_2C) was obtained in the presence of the silica stabilizer and at a synthesis temperature of 680 °C. The observation that SiO_2 stabilizes high-surface-area tungsten carbide and in particular the W_2C-phase shows the importance of investigating the influence of oxide stabilizers and supports in the preparation of tungsten carbide catalysts. The DOE approach represents progress in applying mathematical tools to catalysis research and solid-state synthesis, and the model was successfully extended beyond its original boundaries.

Analysis of powder X-ray diffractograms showed that the W_2C phase was characterized by smaller crystalline domain sizes than the WC phase. This finding confirms the hypothesis that W_2C, usually considered metastable, can become the thermodynamically favorable phase at small particle sizes, that is, at high surface areas. If the surface energy term prevails, then W_2C with its lower surface energy is more favorable than WC although its (bulk) crystal energy is higher relative to WC. The critical domain size identified for the phase change, around 10 nm, is in perfect agreement with the predictions from DFT calculations by Shrestha et al. [33]. The role of particle size for phase stability explains the importance of the silica stabilizer, which disperses the tungsten phase.

The materials were found to be active for hydrogenation of butyraldehyde to butanol and for hydrogenation of toluene to methylcyclohexane. The isothermally synthesized silica-stabilized catalysts possess higher phase purity and increased aldehyde conversion activity compared with materials obtained via the temperature-programmed synthesis method.

The hydrogenation rate for either reaction per total moles tungsten increased with increasing W_2C-content, as did the amount of CO adsorbed. WC did not exhibit many sites for CO adsorption and presumably did not contribute significantly to hydrogenation catalysis. The 1-butanol formation rate was found to be perfectly proportional to the number of sites probed by CO for a set of samples with varying phase composition, indicating that CO captures the active sites well. The correlation for the methylcyclohexane formation rate with CO-counted sites was not perfectly

linear, perhaps reflecting that ensemble sites are needed for aromatic ring hydrogenation. Overall, the variation of turnover frequency with changing phase composition was small.

5. Acknowledgement

The authors thank the German Academic Exchange Service (DAAD, Project-ID: 57510376) and the Deutsche Forschungsgemeinschaft (DFG KO1458/9-1 AOBJ: 630207) for financial support. P.B. thanks the TUM Graduate School and Technical University of Munich for financial support. We want to thank Prof. Dr.-Ing. O. Hinrichsen for providing the equipment for CO chemisorption measurements and Andrea Abram for performing Raman spectroscopy measurements. We also want to thank Prof. Dr. Petra Mela and Theresa Fischer for providing access to their light microscope. This work was, in part, supported by NSF award 1726578 (MRI award for X-ray diffractometer).

6. References

[1] J.H. Sinfelt, D.J.C. Yates, Effect of Carbiding on the Hydrogenolysis Activity of Molybdenum, Nature Physical Science. 229 (1971) 27–28. https://doi.org/10.1038/physci229027b0.

[2] R.B. Levy, M. Boudart, Platinum-Like Behavior of Tungsten Carbide in Surface Catalysis, Science. 181 (1973) 547–549. https://doi.org/10.1126/science.181.4099.547.

[3] Mineral commodity summaries 2021, U.S. Geological Survey, Reston, VA, 2021. https://doi.org/10.3133/mcs2021.

[4] F. Ribeiro, R. Betta, M. Boudart, J. Baumgartner, E. Iglesia, Reactions of neopentane, methylcyclohexane, and 3,3-dimethylpentane on tungsten carbides: The effect of surface oxygen on reaction pathways, J. Catal. 130 (1991) 86–105. https://doi.org/10.1016/0021-9517(91)90094-K.

[5] F.H. Ribeiro, M. Boudart, R.A. Dalla Betta, E. Iglesia, Catalytic reactions of n-Alkanes on β-W2C and WC: The effect of surface oxygen on reaction pathways, Journal of Catalysis. 130 (1991) 498–513. https://doi.org/10.1016/0021-9517(91)90131-M.

[6] J.S. Lee, M. Boudart, Reactivity of tungsten carbides I. Catalytic and temperature-programmed reactions of methanol, Catal Lett. 8 (1991) 107–114. https://doi.org/10.1007/BF00764106.

[7] S.A.W. Hollak, R.W. Gosselink, D.S. van Es, J.H. Bitter, Comparison of Tungsten and Molybdenum Carbide Catalysts for the Hydrodeoxygenation of Oleic Acid, ACS Catal. 3 (2013) 2837–2844. https://doi.org/10.1021/cs400744y.

[8] R.W. Gosselink, D.R. Stellwagen, J.H. Bitter, Tungsten-Based Catalysts for Selective Deoxygenation, Angew. Chem. Int. Ed. 52 (2013) 5089–5092. https://doi.org/10.1002/anie.201209809.

[9] D.R. Stellwagen, J.H. Bitter, Structure–performance relations of molybdenum- and tungsten carbide catalysts for deoxygenation, Green Chem. 17 (2015) 582–593. https://doi.org/10.1039/C4GC01831A.

[10] L. Souza Macedo, V. Teixeira da Silva, J. Bitter, Activated Carbon, Carbon Nanofibers and Carbon-Covered Alumina as Support for W_2C in Stearic Acid Hydrodeoxygenation, ChemEngineering. 3 (2019) 24. https://doi.org/10.3390/chemengineering3010024.

[11] A.L. Jongerius, R.W. Gosselink, J. Dijkstra, J.H. Bitter, P.C.A. Bruijnincx, B.M. Weckhuysen, Carbon Nanofiber Supported Transition-Metal Carbide Catalysts for the Hydrodeoxygenation of Guaiacol, ChemCatChem. 5 (2013) 2964–2972. https://doi.org/10.1002/cctc.201300280.

[12] H. Ren, Y. Chen, Y. Huang, W. Deng, D. G. Vlachos, J. G. Chen, Tungsten carbides as selective deoxygenation catalysts: experimental and computational studies of converting C3 oxygenates to propene, Green Chemistry. 16 (2014) 761–769. https://doi.org/10.1039/C3GC41256C.

[13] A. Wang, T. Zhang, One-Pot Conversion of Cellulose to Ethylene Glycol with Multifunctional Tungsten-Based Catalysts, Acc. Chem. Res. 46 (2013) 1377–1386. https://doi.org/10.1021/ar3002156.

[14] R. Ooms, M. Dusselier, J.A. Geboers, B. Op de Beeck, R. Verhaeven, E. Gobechiya, J.A. Martens, A. Redl, B.F. Sels, Conversion of sugars to ethylene glycol with nickel tungsten carbide in a fed-batch reactor: high productivity and reaction network elucidation, Green Chem. 16 (2014) 695–707. https://doi.org/10.1039/C3GC41431K.

[15] H. Guo, B. Zhang, C. Li, C. Peng, T. Dai, H. Xie, A. Wang, T. Zhang, Tungsten Carbide: A Remarkably Efficient Catalyst for the Selective Cleavage of Lignin C−O Bonds, ChemSusChem. 9 (2016) 3220–3229. https://doi.org/10.1002/cssc.201600901.

[16] P. Bretzler, M. Huber, S. Nickl, K. Köhler, Hydrogenation of furfural by noble metal-free nickel modified tungsten carbide catalysts, RSC Adv. 10 (2020) 27323–27330. https://doi.org/10.1039/D0RA02003F.

[17] D.V. Esposito, S.T. Hunt, Y.C. Kimmel, J.G. Chen, A New Class of Electrocatalysts for Hydrogen Production from Water Electrolysis: Metal Monolayers Supported on Low-Cost Transition Metal Carbides, J. Am. Chem. Soc. 134 (2012) 3025–3033. https://doi.org/10.1021/ja208656v.

[18] Y.-J. Ko, J.-M. Cho, I. Kim, D.S. Jeong, K.-S. Lee, J.-K. Park, Y.-J. Baik, H.-J. Choi, W.-S. Lee, Tungsten carbide nanowalls as electrocatalyst for hydrogen evolution reaction: New approach to durability issue, Applied Catalysis B: Environmental. 203 (2017) 684–691. https://doi.org/10.1016/j.apcatb.2016.10.085.

[19] L.-N. Zhang, Y.-Y. Ma, Z.-L. Lang, Y.-H. Wang, S.U. Khan, G. Yan, H.-Q. Tan, H.-Y. Zang, Y. Li, Ultrafine cable-like WC/W_2C heterojunction nanowires covered by graphitic carbon

towards highly efficient electrocatalytic hydrogen evolution, J. Mater. Chem. A. 6 (2018) 15395–15403. https://doi.org/10.1039/C8TA05007D.

[20] S. Meyer, A.V. Nikiforov, I.M. Petrushina, K. Köhler, E. Christensen, J.O. Jensen, N.J. Bjerrum, Transition metal carbides (WC, Mo_2C, TaC, NbC) as potential electrocatalysts for the hydrogen evolution reaction (HER) at medium temperatures, International Journal of Hydrogen Energy. 40 (2015) 2905–2911. https://doi.org/10.1016/j.ijhydene.2014.12.076.

[21] P. Bretzler, K. Köhler, A.V. Nikiforov, E. Christensen, R.W. Berg, N.J. Bjerrum, Efficient water splitting electrolysis on a platinum-free tungsten carbide electrocatalyst in molten CsH_2PO_4 at 350–390 °C, International Journal of Hydrogen Energy. 45 (2020) 21262–21272. https://doi.org/10.1016/j.ijhydene.2020.05.145.

[22] L. Volpe, M. Boudart, Compounds of molybdenum and tungsten with high specific surface area, Journal of Solid State Chemistry. 59 (1985) 348–356. https://doi.org/10.1016/0022-4596(85)90302-0.

[23] F.H. Ribeiro, R.A. Dalla Betta, G.J. Guskey, M. Boudart, Preparation and surface composition of tungsten carbide powders with high specific surface area, Chem. Mater. 3 (1991) 805–812. https://doi.org/10.1021/cm00017a015.

[24] G. Leclercq, M. Kamal, J.M. Giraudon, P. Devassine, L. Feigenbaum, L. Leclercq, A. Frennet, J.M. Bastin, A. Löfberg, S. Decker, M. Dufour, Study of the Preparation of Bulk Powder Tungsten Carbides by Temperature Programmed Reaction with CH_4 + H_2 Mixtures, Journal of Catalysis. 158 (1996) 142–169. https://doi.org/10.1006/jcat.1996.0015.

[25] A. Löfberg, A. Frennet, G. Leclercq, L. Leclercq, J.M. Giraudon, Mechanism of WO_3 Reduction and Carburization in CH_4/H_2 Mixtures Leading to Bulk Tungsten Carbide Powder Catalysts, Journal of Catalysis. 189 (2000) 170–183. https://doi.org/10.1006/jcat.1999.2692.

[26] T. Xiao, A. Hanif, A.P.E. York, J. Sloan, M.L.H. Green, Study on preparation of high surface area tungsten carbides and phase transition during the carburisation, Phys. Chem. Chem. Phys. 4 (2002) 3522–3529. https://doi.org/10.1039/b202518c.

[27] A.S. Kurlov, A.I. Gusev, Tungsten carbides and W-C phase diagram, Inorg Mater. 42 (2006) 121–127. https://doi.org/10.1134/S0020168506020051.

[28] K.M. Reddy, T.N. Rao, J. Joardar, Stability of nanostructured W-C phases during carburization of WO3, Materials Chemistry and Physics. 128 (2011) 121–126. https://doi.org/10.1016/j.matchemphys.2011.02.045.

[29] G. Leclercq, M. Kamal, J.-F. Lamonier, L. Feigenbaum, P. Malfoy, L. Leclercq, Treatment of bulk group VI transition metal carbides with hydrogen and oxygen, Applied Catalysis A: General. 121 (1995) 169–190. https://doi.org/10.1016/0926-860X(94)00203-7.

[30] T. Ishii, K. Yamada, N. Osuga, Y. Imashiro, J. Ozaki, Single-Step Synthesis of W_2C Nanoparticle-Dispersed Carbon Electrocatalysts for Hydrogen Evolution Reactions Utilizing Phosphate Groups on Carbon Edge Sites, ACS Omega. 1 (2016) 689–695. https://doi.org/10.1021/acsomega.6b00179.

[31] Q. Gong, Y. Wang, Q. Hu, J. Zhou, R. Feng, P.N. Duchesne, P. Zhang, F. Chen, N. Han, Y. Li, C. Jin, Y. Li, S.-T. Lee, Ultrasmall and phase-pure W_2C nanoparticles for efficient electrocatalytic and photoelectrochemical hydrogen evolution, Nat Commun. 7 (2016) 13216. https://doi.org/10.1038/ncomms13216.

[32] D.V. Suetin, I.R. Shein, A.L. Ivanovskii, Structural, electronic properties and stability of tungsten mono- and semi-carbides: A first principles investigation, Journal of Physics and Chemistry of Solids. 70 (2009) 64–71. https://doi.org/10.1016/j.jpcs.2008.09.004.

[33] A. Shrestha, X. Gao, J.C. Hicks, C. Paolucci, Nanoparticle Size Effects on Phase Stability for Molybdenum and Tungsten Carbides, Chem. Mater. 33 (2021) 4606–4620. https://doi.org/10.1021/acs.chemmater.1c01120.

[34] C. Li, M. Zheng, A. Wang, T. Zhang, One-pot catalytic hydrocracking of raw woody biomass into chemicals over supported carbide catalysts: simultaneous conversion of cellulose, hemicellulose and lignin, Energy Environ. Sci. 5 (2012) 6383–6390. https://doi.org/10.1039/C1EE02684D.

[35] H. Fang, J. Du, C. Tian, J. Zheng, X. Duan, L. Ye, Y. Yuan, Regioselective hydrogenolysis of aryl ether C–O bonds by tungsten carbides with controlled phase compositions, Chem. Commun. 53 (2017) 10295–10298. https://doi.org/10.1039/C7CC05487D.

[36] H. Fang, A. Roldan, C. Tian, Y. Zheng, X. Duan, K. Chen, L. Ye, S. Leoni, Y. Yuan, Structural tuning and catalysis of tungsten carbides for the regioselective cleavage of C O bonds, Journal of Catalysis. 369 (2019) 283–295. https://doi.org/10.1016/j.jcat.2018.11.020.

[37] R. Liu, M. Pang, X. Chen, C. Li, C. Xu, C. Liang, W $_2$ C nanorods with various amounts of vacancy defects: determination of catalytic active sites in the hydrodeoxygenation of benzofuran, Catal. Sci. Technol. 7 (2017) 1333–1341. https://doi.org/10.1039/C6CY02702D.

[38] S.T. Hunt, T. Nimmanwudipong, Y. Román-Leshkov, Engineering Non-sintered, Metal-Terminated Tungsten Carbide Nanoparticles for Catalysis, Angew. Chem. Int. Ed. 53 (2014) 5131–5136. https://doi.org/10.1002/anie.201400294.

[39] S.T. Hunt, M. Milina, A.C. Alba-Rubio, C.H. Hendon, J.A. Dumesic, Y. Roman-Leshkov, Self-assembly of noble metal monolayers on transition metal carbide nanoparticle catalysts, Science. 352 (2016) 974–978. https://doi.org/10.1126/science.aad8471.

[40] L. Hu, S. Ji, T. Xiao, C. Guo, P. Wu, P. Nie, Preparation and Characterization of Tungsten Carbide Confined in the Channels of SBA-15 Mesoporous Silica, J. Phys. Chem. B. 111 (2007) 3599–3608. https://doi.org/10.1021/jp066349b.

[41] L. Hu, S. Ji, Z. Jiang, H. Song, P. Wu, Q. Liu, Direct Synthesis and Structural Characteristics of Ordered SBA-15 Mesoporous Silica Containing Tungsten Oxides and Tungsten Carbides, J. Phys. Chem. C. 111 (2007) 15173–15184. https://doi.org/10.1021/jp074879h.

[42] M.G. Álvarez, R.J. Chimentão, D. Tichit, J.B.O. Santos, A. Dafinov, L.B. Modesto-López, J. Rosell-Llompart, E.J. Güell, F. Gispert-Guirado, J. Llorca, F. Medina, Synthesis of tungsten carbide on Al-SBA-15 mesoporous materials by carburization, Microporous and Mesoporous Materials. 219 (2016) 19–28. https://doi.org/10.1016/j.micromeso.2015.07.018.

[43] Y. Liu, L. Zhang, F. Göltl, M.R. Ball, I. Hermans, T.F. Kuech, M. Mavrikakis, J.A. Dumesic, Synthesis Gas Conversion over Rh-Mn-W_xC/SiO_2 Catalysts Prepared by Atomic Layer Deposition, ACS Catal. 8 (2018) 10707–10720. https://doi.org/10.1021/acscatal.8b02461.

[44] J.M. McHale, Surface Energies and Thermodynamic Phase Stability in Nanocrystalline Aluminas, Science. 277 (1997) 788–791. https://doi.org/10.1126/science.277.5327.788.

[45] H. Zhang, J.F. Banfield, Thermodynamic analysis of phase stability of nanocrystalline titania, J. Mater. Chem. 8 (1998) 2073–2076. https://doi.org/10.1039/a802619j.

[46] B.S. Klose-Schubert, R.E. Jentoft, F.C. Jentoft, The balance between reactivity and stability of modified oxide surfaces illustrated by the behavior of sulfated zirconia catalysts, Top Catal. 54 (2011) 398–414. https://doi.org/10.1007/s11244-011-9670-5.

[47] A. Mehdad, R.E. Jentoft, F.C. Jentoft, Single-phase mixed molybdenum-tungsten carbides: Synthesis, characterization and catalytic activity for toluene conversion, Catalysis Today. 323 (2019) 112–122. https://doi.org/10.1016/j.cattod.2018.06.037.

[48] E. Iglesia, F.H. Ribeiro, M. Boudart, J.E. Baumgartner, Synthesis, characterization, and catalytic properties of clean and oxygen-modified tungsten carbides, Catalysis Today. 15 (1992) 307–337. https://doi.org/10.1016/0920-5861(92)80181-L.

[49] M.J. Anderson, P.J. Whitcomb, DOE simplified: practical tools for effective experimentation, 2nd ed, Productivity Press, New York, N.Y, 2007.

[50] V.V. Pushkarev, K. An, S. Alayoglu, S.K. Beaumont, G.A. Somorjai, Hydrogenation of benzene and toluene over size controlled Pt/SBA-15 catalysts: Elucidation of the Pt particle size effect on reaction kinetics, Journal of Catalysis. 292 (2012) 64–72. https://doi.org/10.1016/j.jcat.2012.04.022.

[51] P.S.F. Mendes, G. Lapisardi, C. Bouchy, M. Rivallan, J.M. Silva, M.F. Ribeiro, Hydrogenating activity of Pt/zeolite catalysts focusing acid support and metal dispersion influence, Applied Catalysis A: General. 504 (2015) 17–28. https://doi.org/10.1016/j.apcata.2015.03.027.

[52] M.B. Fichtl, O. Hinrichsen, On the Temperature Programmed Desorption of Hydrogen from Polycrystalline Copper, Catal Lett. 144 (2014) 2114–2120. https://doi.org/10.1007/s10562-014-1384-4.

[53] M.-L. Frauwallner, F. López-Linares, J. Lara-Romero, C.E. Scott, V. Ali, E. Hernández, P. Pereira-Almao, Toluene hydrogenation at low temperature using a molybdenum carbide catalyst, Applied Catalysis A: General. 394 (2011) 62–70. https://doi.org/10.1016/j.apcata.2010.12.024.

[54] A. Mehdad, R.E. Jentoft, F.C. Jentoft, Single-phase mixed molybdenum-niobium carbides: Synthesis, characterization and multifunctional catalytic behavior in toluene conversion, Journal of Catalysis. 351 (2017) 161–173. https://doi.org/10.1016/j.jcat.2017.04.022.

[55] W.P. Davey, Precision Measurements of the Lattice Constants of Twelve Common Metals, Phys. Rev. 25 (1925) 753–761. https://doi.org/10.1103/PhysRev.25.753.

[56] E. Parthé, V. Sadagopan, Neutronen- und Röntgenbeugungsuntersuchungen über die Struktur des Wolframcarbides WC und Vergleich mit älteren Elektronenbeugungsdaten, Monatshefte für Chemie. 93 (1962) 263–270. https://doi.org/10.1007/BF00908251.

[57] M.C. Morris, H.F. McMurdie, E.H. Evans, B. Paretzkin, H.S. Parker, W. Wong-Ng, D.M. Gladhill, C.R. Hubbard, Standard X-ray diffraction powder patterns, (1985).

[58] A.S. Kurlov, A.I. Gusev, Neutron and x-ray diffraction study and symmetry analysis of phase transformations in lower tungsten carbide W_2C, Phys. Rev. B. 76 (2007) 174115. https://doi.org/10.1103/PhysRevB.76.174115.

[59] H. Zhuang, A.J. Tkalych, E.A. Carter, Surface Energy as a Descriptor of Catalytic Activity, J. Phys. Chem. C. 120 (2016) 23698–23706. https://doi.org/10.1021/acs.jpcc.6b09687.

[60] D.K. Gupta, L.L. Seigle, Free energies of formation of WC and W2C, and the thermodynamic properties of carbon in solid tungsten, MTA. 6 (1975) 1939–1944. https://doi.org/10.1007/BF02646859.

[61] A.A. Koverga, E. Flórez, L. Dorkis, J.A. Rodriguez, CO, CO_2, and H_2 Interactions with (0001) and (001) Tungsten Carbide Surfaces: Importance of Carbon and Metal Sites, The Journal of Physical Chemistry C. (2019). https://doi.org/10.1021/acs.jpcc.8b11840.

[62] D.R. McIntyre, G.T. Burstein, A. Vossen, Effect of carbon monoxide on the electrooxidation of hydrogen by tungsten carbide, Journal of Power Sources. 107 (2002) 67–73. https://doi.org/10.1016/S0378-7753(01)00987-9.

[63] Z.J. Mellinger, T.G. Kelly, J.G. Chen, Pd-Modified Tungsten Carbide for Methanol Electro-oxidation: From Surface Science Studies to Electrochemical Evaluation, ACS Catal. 2 (2012) 751–758. https://doi.org/10.1021/cs200620x.

[64] J. Brillo, R. Sur, H. Kuhlenbeck, H.-J. Freund, Interaction of CO and NO with WC(0001), Surface Science. 397 (1998) 137–144. https://doi.org/10.1016/S0039-6028(97)00725-5.